Supporting information

NIR-II absorption and photothermal conversion in a photochromic metal-organic framework based on *cis*-2,2'-biquinoline-4,4'-dicarboxylate

Ning-Ning Zhang[a], Ya-Ru Li[a], Li Li[c], Wei-Li Zheng[a], Lin-Xu Liu[a], Zhen-Yu Li[b,d], Yunyun Dong[a], Jinsheng Zhao[a,*], Kong-Gang Qu[a,*] and Yong Yan[a,d,*]

[a]*School of Chemistry and Chemical Engineering, Liaocheng University, Liaocheng, Shandong 252000, P. R. China.*

[b]*School of Environmental and Materials Engineering, Yantai University, Yantai, 264005, P. R. China.*

[c]*School of Materials Science and Engineering, Henan Polytechnic University, Jiaozuo, 454000, P. R. China.*

[d]*State Key Laboratory of Structural Chemistry, Fujian Institute of Research on the Structure of Matter, Chinese Academy of Sciences, Fuzhou, Fujian 350002, P. R. China.*

**Email: j.s.zhao@163.com (J. Zhao); qukonggang@lcu.edu.cn (K. G. Qu); yanyong1036@gmail.com (Y. Yan).*

1. Experimental section

1.1 General methods

1). Infrared (IR) data were collected using a Nicolet iS50 FT-IR spectrophotometer, covering the range from 4000−400 cm^{-1} with air as the baseline.

2). Electronic absorption spectra were obtained in the reflectance mode at room temperature using a UH4150 spectrophotometer equipped with an integrating sphere attachment, and pure $BaSO_4$ served as the baseline.

3). Solid-state electron paramagnetic resonance (EPR) spectra were recorded on an EPR-200Plus electron paramagnetic resonance spectrometer operating at a magnetic field of 100 kHz in the X band.

4). Powder X-ray diffraction (PXRD) patterns were collected at room temperature using a SmartLab 9 Kw diffractometer using Cu K_α radiation (λ = 1.5406 Å, 450 W). Simulated PXRD patterns generated using Mercury Version 3.5.1 software based on X-ray single crystal diffraction data.

5). Photoluminescence spectra were measured using an FLS1000 phosphorimeter with a 450W Xenon lamp as excitation source.

6). Light source of photochromism: CEL-PF300-T9 xenon lamp system was used to illuminate samples for achieving various spectra. The voltage was 15V and the current was set to 16A, so the used power was 240W. Then, the distance between the sample and the Xe lamp was around 20 cm.

7). The NRI-II photothermal conversion measurement were conducted by irradiating crystalline plates with a 1064 nm Xinchanye laser. Sample temperatures were monitored using a HIKMICRO K20 infrared camera equipped with a micromirror. The crystalline plates were prepared with a tablet pressing machine with a diameter of 5 mm. The weight of the plate is 7 mg for NRI-II photothermal conversion measurement.

8). Thermogravimetry (TG) and differential scanning calorimetry (DSC) analyses were performed using a Netzsch STA449F3 simultaneous thermal analyzer with Al_2O_3 crucibles under N_2 (20 mL min^{-1}) at a heating rate of 10 K min^{-1} over the range of 30–800 °C.

1.2 Computational details

1). The DOS was calculated using the CASTEP package[1] in Materials studio 8.0. The structural model for compound **1** was built directly from the single-crystal X-ray diffraction data. The exchange-correlation energy was described by the PBE functional within the GGA.[2,3] The norm conserving pseudopotentials were chosen to modulate the electron−ion interaction.[4,5] The

plane-wave cut off energy was 750 eV, and the threshold of 5×10^{-7} eV was set for the self-consistent field convergence of the total electronic energy. The Fermi level was selected as the reference and set to 0 eV by default. The smearing width was set to 0.05 eV for DOS. Other parameters were set to default values.

2). Calculation of intermolecular interactions[6] in **1**: The plots of the electron density (ρ), reduced density gradient ($s = 1/(2(3\pi^2)^{1/3})|\nabla\rho|/\rho^{4/3}$) were obtained by density functional theory calculations. Calculations were performed with the B3LYP[7] functional and the 6-311G (d,p) basis set, using the Gaussian 16 program[8]. The results were analyzed by Multiwfn[9] and VMD.

3). Calculation of theoretical UV-Vis absorption spectra and spin density. The mode of monomer radical ([BCA]$^{\bullet\bullet}$), dimer radicals (2[BCA]$^{\bullet\bullet}$) and trimer radicals (3[BCA]$^{\bullet\bullet}$) were directly built from crystal structure data of **1**. Time-dependent density functional theory (TD-DFT) calculations were performed with the m062X functional and the 6-311G (d,p) basis set, using the Gaussian 16 program[8]. The results of UV-Vis absorption spectrum and molecular orbitals were analyzed by Multiwfn[9]. The spin density result was obtained from GaussView 5.0.

1.3 Materials and Synthesis

Materials. All chemical reagents and solvents utilized in the synthetic experiments were of analytical grade and required no further purification.

Synthesis of compound 1. Compound **1** was synthesized using revised documentation procedures[10], resulting in simplified synthesis procedures. For the preparation of **1** ($\{[Cd(BCA)]_2\cdot(H_2O)_2\cdot DMF\}_n$), a mixture comprising $Cd(NO_3)_2$ (0.2 mmol, 61.6 mg), BCA (0.1 mmol, 35 mg), 4 mL DMF was transferred into a 10 mL Teflon lined autoclave and sealed. The reaction proceeded at 110 °C for 3 day, yielding light yellow crystalline samples. These samples were collected after filtration (yield: ~65 % based on BCA ligand). The phase purity of **1** was confirmed by IR (Fig. S1) and PXRD data (Fig. S2).

2. Additional graphics

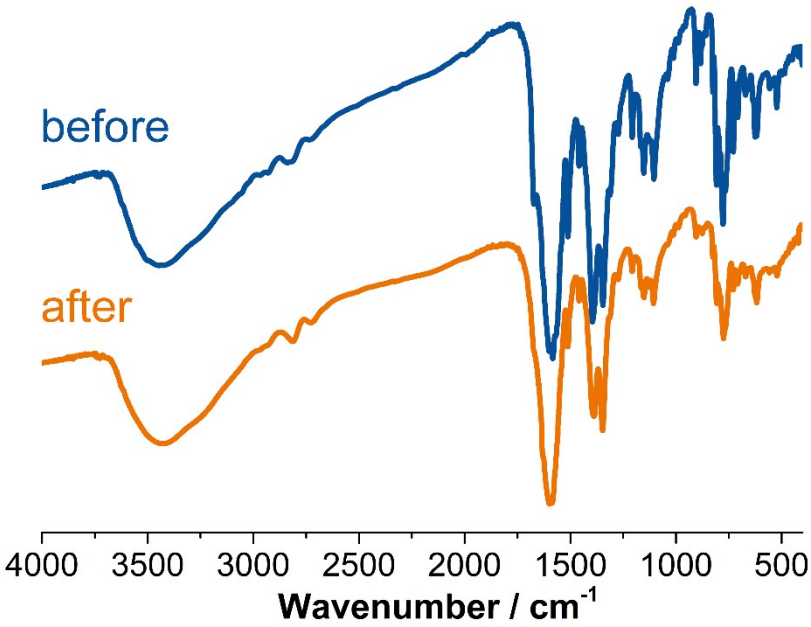

Fig. S1 IR spectra of compound 1: before, measured data for as-synthesized samples; after, measured data for colored samples.

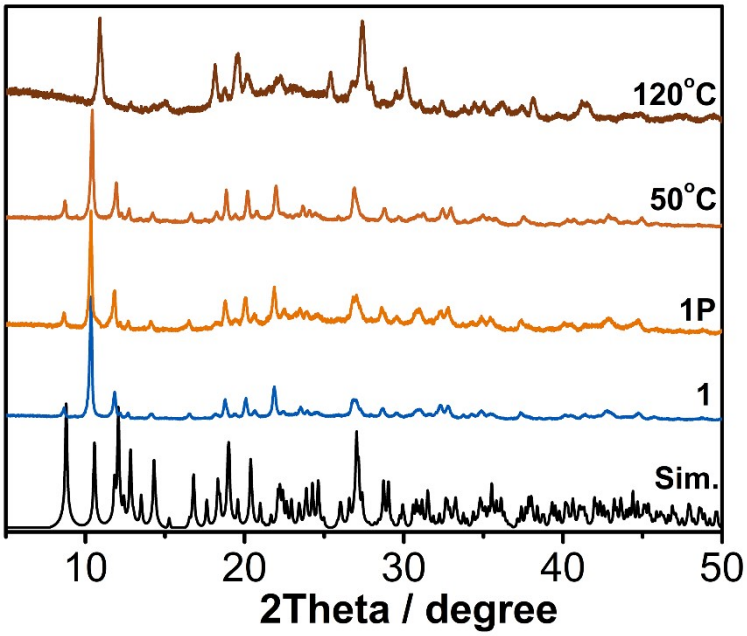

Fig. S2 PXRD patterns of compound **1** and **1P**. Sim.: simulated data using single-crystal data. And the data for **1P** samples after annealing at 50 °C and 120 °C for 2 hours are also shown.

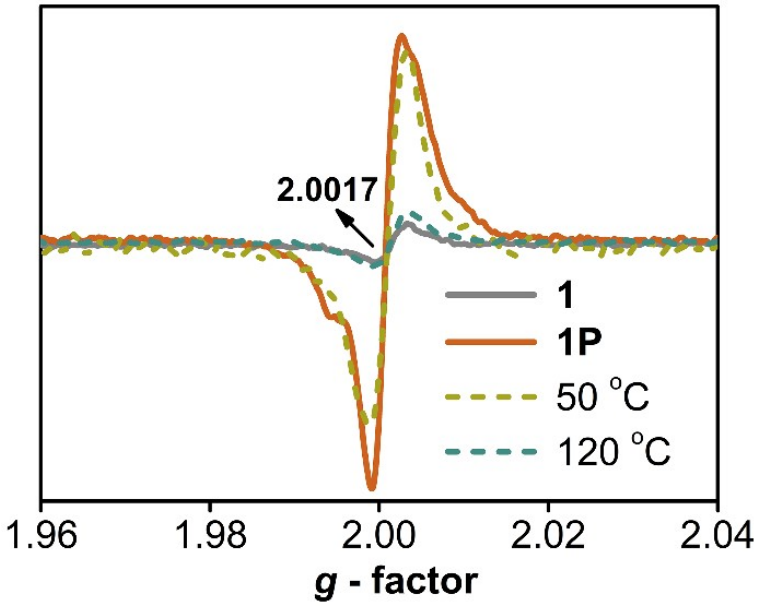

Fig. S3 EPR spectra of **1** and **1P** in the solid state. And the data for **1P** samples after annealing at 50 °C and 120 °C for 2 hours are also shown.

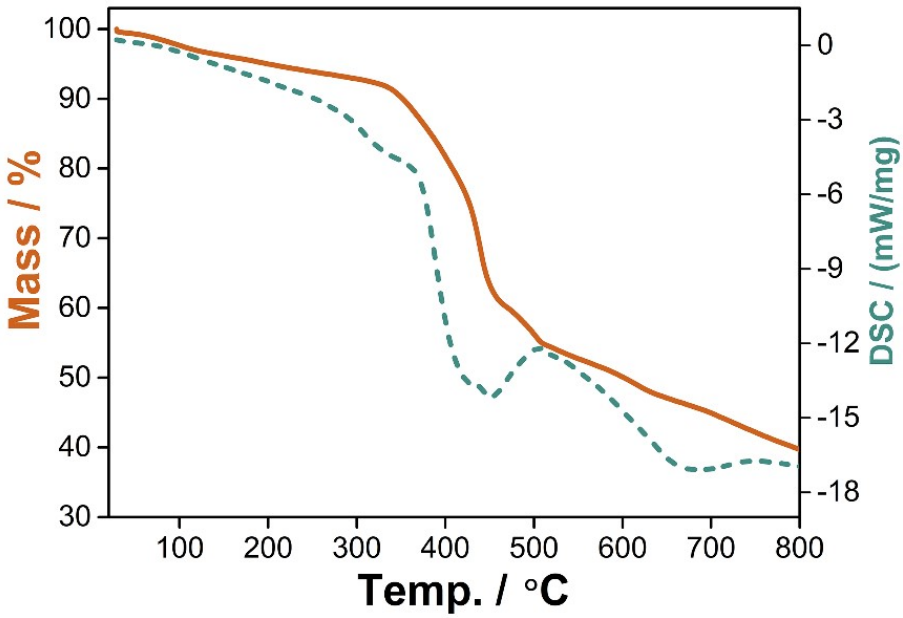

Fig. S4 The thermogravimetric (orange solid line) and differential scanning calorimetric (green dotted line) curves for metal-organic framework **1**.

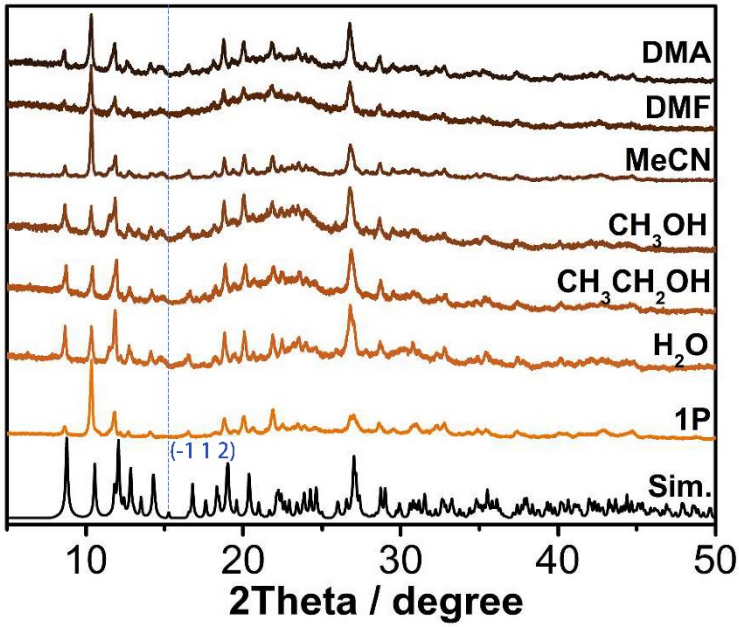

Fig. S5 PXRD patterns of **1P**. Sim.: simulated data using single-crystal data. And the data for **1P** samples after immersing in different solvents for 1 day are also shown. Compared to the simulated pattern at 100 K, the slight blue shift in the diffraction peak at 15.3°, corresponding to the (-1 1 2) plane, is likely attributed to minor structural expansion at room temperature.

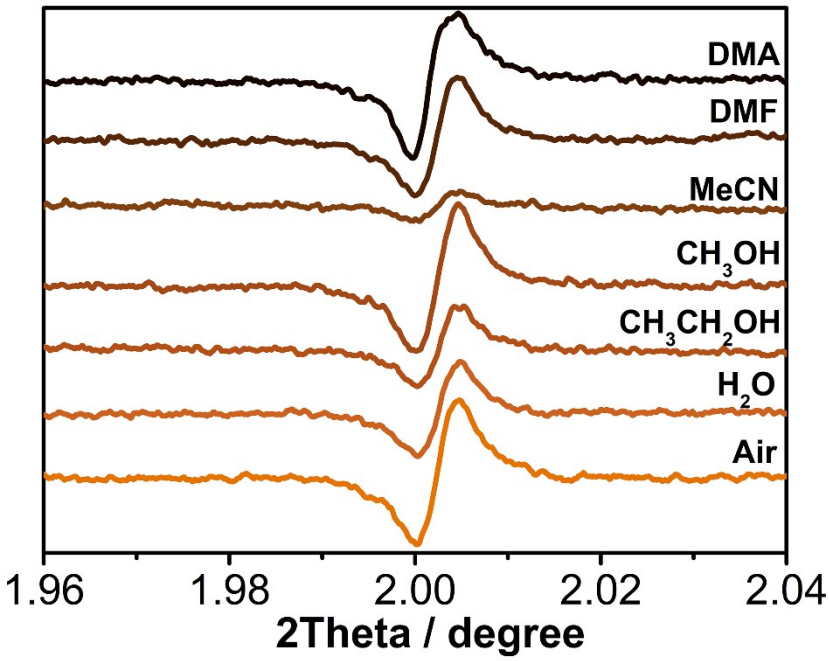

Fig. S6 Solid-state EPR spectra of **1P** placed in air and immersed in various solvents for 1 day (same test conditions and sample weight).

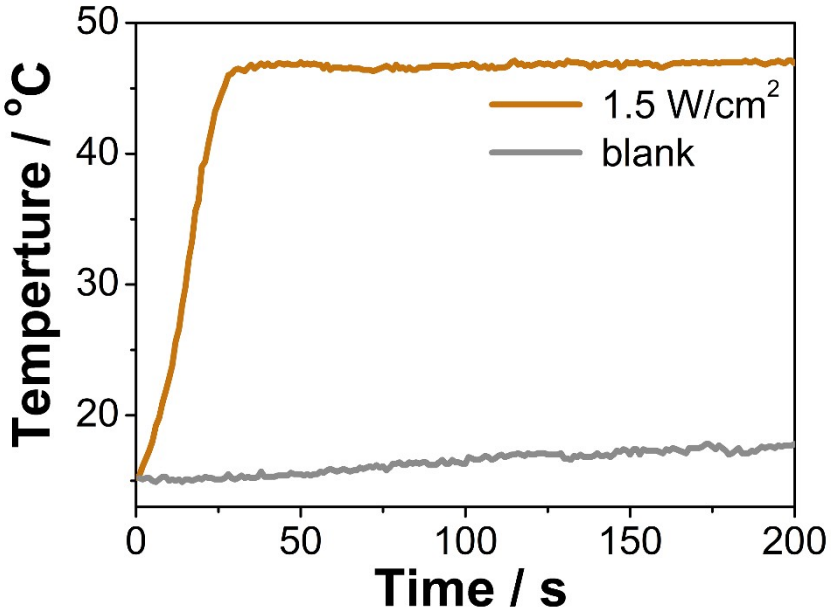

Fig. S7 Temperature curves of **1P** and blank quartz glass plate under the irradiation of a 1.5 W/cm^2 1064 nm laser.

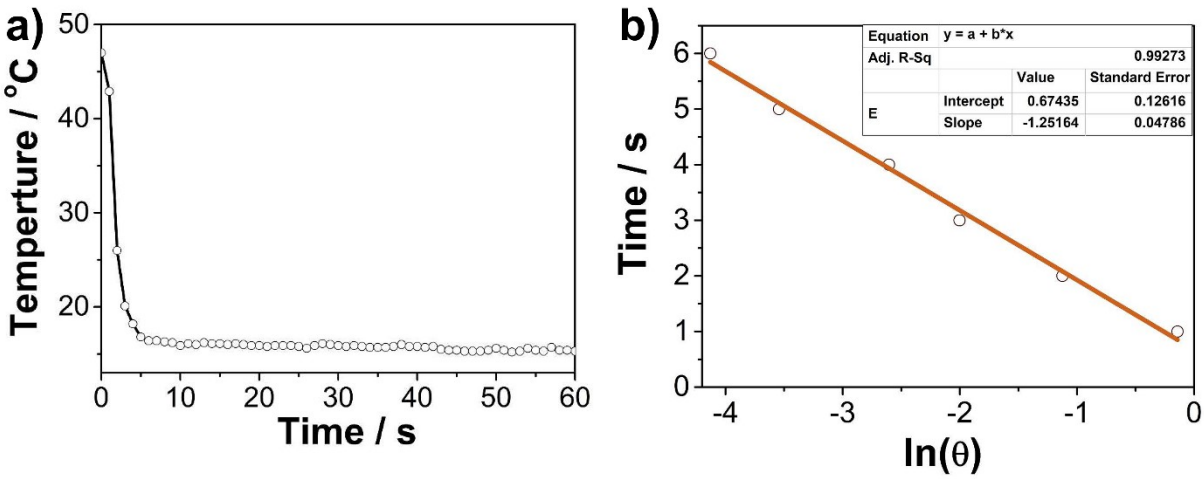

Fig. S8 Temperature decaying curve of compound **1P** after removing the laser source of 1064 nm (1.5 W/cm^2) (a) and the corresponding time-lnθ linear curve (b). The photothermal conversion efficiency (η_{1064} = 54.27 %) was also calculated based on reported method[11]: $\eta_{1064} = \frac{hS\Delta T_{max}}{I(1-10^{-A_{1064}})}$, where the I is the laser power (1.5 W/cm^2), A_{1064} is the absorbance of the samples at the wavelength of 1064 nm (0.14, F(R)), and ΔT_{max} is the maximum temperature change (35.5 K). hs can be calculated based on the formula of $\tau_s = \frac{\sum_i m_i C_{p,i}}{hs}$, where τ_s is the

sample system time constant, m_i (0.007 g) and $C_{p,i}$ (1.13 J·(g·°C)$^{-1}$) are the mass and heat capacity of system components. When the laser turns off, τ_s can be estimated according to the formula: $t = -\tau_s \ln\theta$. The θ can be obtained according to the formula: $\theta = \frac{T - T_{surr}}{T_{max} - T_{surr}}$, where T is the temperature of sample, T_{max} is the maximum system temperature, and T_{surr} is the environment temperature.

3. References

1 S. J. Clark, M. D. Segall, C. J. Pickard, P. J. Hasnip, M. I. J. Probert, K. Refson, M. C. Payne, First principles methods using CASTEP. *Z Kristallogr-Cryst Mater,* 2005, **220**, 567−570.

2 B. Hammer, L. B. Hansen, J. K. Norskov, Improved adsorption energetics within density-functional theory using revised Perdew-Burke-Ernzerhof functionals. *Phys. Rev. B Condens Matter Mater Phys.,* 1999, **59**, 7413−7421.

3 J. P. Perdew, Y. Wang, Accurate and simple analytic representation of the electron-gas correlation energy. *Phys Rev B Condens Matter Mater Phys,* 1992, **45**, 13244−13249.

4 D. R. Hamann, M. Schlüter, C. Chiang, Norm-Conserving Pseudopotentials. *Phys. Rev. Lett*., 1979, **43**, 1494−1497.

5 J. S. Lin, A. Qteish, M. C. Payne, V. Heine, Optimized and transferable nonlocal separable ab initio pseudopotentials. *Phys. Rev. B Condens Matter Mater Phys.,* 1993, **47**, 4174−4180.

6 E. R. Johnson, S. Keinan, P. Mori-Sánchez, J. Contreras-García, A. J. Cohen, W. Yang, Revealing noncovalent interactions, *J. Am. Chem. Soc.*, 2010, **132**, 6498–6506.

7 L. A. Curtiss, P. C. Redfern, K. Raghavachari, J. A. Pople, Gaussian-3X (G3X) theory: Use of improved geometries, zero-point energies, and Hartree–Fock basis sets. *J. Chem. Phys.* 2001, **114**, 108−117.

8 Gaussian 16, Revision C.01, M. J. Frisch, G. W. Trucks, H. B. Schlegel, G. E. Scuseria, M. A. Robb, J. R. Cheeseman, G. Scalmani, V. Barone, G. A. Petersson, H. Nakatsuji, X. Li, M. Caricato, A. V. Marenich, J. Bloino, B. G. Janesko, R. Gomperts, B. Mennucci, H. P. Hratchian, J. V. Ortiz, A. F. Izmaylov, J. L. Sonnenberg, D. Williams-Young, F. Ding, F. Lipparini, F. Egidi, J. Goings, B. Peng, A. Petrone, T. Henderson, D. Ranasinghe, V. G. Zakrzewski, J. Gao, N. Rega, G. Zheng, W. Liang, M. Hada, M. Ehara, K. Toyota, R. Fukuda, J. Hasegawa, M. Ishida, T. Nakajima, Y. Honda, O. Kitao, H. Nakai, T. Vreven, K. Throssell, J. A. Montgomery, Jr., J. E. Peralta, F. Ogliaro, M. J. Bearpark, J. J. Heyd, E. N. Brothers, K. N. Kudin, V. N. Staroverov, T. A. Keith, R. Kobayashi, J. Normand, K. Raghavachari, A. P. Rendell, J. C. Burant, S. S. Iyengar, J. Tomasi, M. Cossi, J. M. Millam, M. Klene, C. Adamo, R. Cammi, J. W. Ochterski, R. L. Martin, K. Morokuma, O. Farkas, J. B. Foresman, and D. J. Fox, Gaussian, Inc., Wallingford CT, 2016.

9 T. Lu and F. W. Chen, Multiwfn: A multifunctional wavefunction analyzer, *J. Comput.*

Chem., 2012, **33**, 580–592.
10 J. M. Pérez, S. Morales-Cámara, F. M. García-Salas, N. RuizCuevas, M. E. López-Vargas, D. Choquesillo-Lazarte, J. Cepeda, J. A. García, V. K. Abdelkader-Fernández, A. Rodríguez-Diéguez, S. Rojas and I. Fernández, Metal−Organic Frameworks Based on a Janus-Head Biquinoline Ligand as Catalysts in the Transformation of Carbonyl Compoundsinto Cyanohydrins and Alcohols, *Cryst. Growth Des.*, 2022, **22**, 7395–7404.
11 S. Wang, S. Li, J. Xiong, Z. Lin, W. Wei and Y. Xu, Near-infrared photothermal conversion of stable radicals photoinduced from a viologen-based coordination polymer, *Chem. Commun.*, 2020, **56**, 7399–7402.